

# Fabrication and Proton Conductivity of Sulfonated Silica Composites Prepared by Postoxidization of Mercaptomethoxysilane

Kazuhiro Yasumoto,<sup>1</sup> Tomohisa Norisuye,<sup>1</sup> Yusuke Teranishi,<sup>1</sup> Qui Tran-Cong-Miyata,<sup>1</sup> Shigeki Nomura<sup>2</sup>

<sup>1</sup>Department of Macromolecular Science and Engineering, Graduate School of Science & Technology, Kyoto Institute of Technology, Matsugasaki, Sakyo-ku, Kyoto 606-8585, Japan

<sup>2</sup>R&D Center, Sekisui Chemical Co., Ltd., 32 Wadai, Tsukuba-shi, Ibaraki 300-4292, Japan

Correspondence to: T. Norisuye (E-mail: nori@kit.jp)

Received 22 September 2011; accepted 12 April 2012; published online

DOI: 10.1002/pola.26109

**ABSTRACT:** Sol–gel derived organic–inorganic hybrids containing phosphotungstic acid (PWA) have been prepared previously to obtain proton conductive membranes. However, leaking of PWA was a serious problem to achieve the higher proton conductivity. In this study, polyelectrolyte membranes functionalized with sulfonic acid groups were fabricated by the sol–gel method. Proton conductivity measurements were performed on an impedance analyzer at 80°C/95% RH. The functionalized polyelectrolyte membranes exhibited the proton conductivity  $\sigma \sim 0.9$  (S/cm) which was much higher than the previously reported hybrids containing PWA. Although the hybrids exhibited fairly high proton conductivity irrespective to the catalysts used, that under the low relative humidity

strongly depends on the catalysts. Among the hybrids prepared in this study, the membrane synthesized with HCl showed outstanding proton conductive properties even at the low humidity thanks to the proton transport channel formed by the swelling of ionic clusters. This fact was confirmed by measuring the ion exchange capacity, water uptake, swelling rate, Fourier transform infrared spectroscopy, atomic force microscopy, and thermogravimetric analysis. © 2012 Wiley Periodicals, Inc. *J Polym Sci Part A: Polym Chem* 000: 000–000, 2012

**KEYWORDS:** atomic force microscopy; heteropolyacid; proton conductivity; sol–gel; inorganic polymers; membranes; nanocomposites; networks; structure-property relations; silicas

**INTRODUCTION** A nano-composite consisting of a flexible organic unit and a rigid inorganic junction provides effective means to preserve functional molecules in network, providing functionalities such as superior thermal and mechanical stabilities compared with conventional polymer films.<sup>1</sup> As an example of such composites, 1, 8-bis(triethoxysilyl)octane (TesOct) containing a moderate length of methylene bridge between two alkoxide groups, enables rapid gelation without intramolecular cyclization<sup>2</sup> and thus can be suitably used as a host to fabricate organic–inorganic hybrid materials. In the previous studies,<sup>3,4</sup> phosphotungstic acid (PWA), a superacid as a catalyst, was effectively doped in the TesOct matrix to obtain proton conductive membranes which exhibited the practically acceptable conductivity  $\sigma \sim 10^{-2}$  (S/cm) although the material was in the amorphous state. The materials has a potential of being used as a crosslinking host for fuel cell applications,<sup>5–11</sup> preventing the chemical short due to a leak of fuels throughout the membrane.

Although the better proton conductivity or thermostability was one of the most important strategies for the fuel cell applications, designing structures at molecular level efficient

for the proton transfer through the continuous phase is strongly demanded. The most popular methods would be (1) manipulating the continuous conductive phase<sup>7,12–18</sup> or (2) forming the condensed ion-clusters by cluster growth.<sup>19,20</sup> The former corresponds to ion-rich continuous structures constructed by a delicate balance between the hydrophobic and hydrophilic interactions as often seen in perfluorinated membranes.<sup>21–25</sup> Conversely, the latter can be obtained by interconnection of the well-developed clusters without macroscopic phase separation.

So far, we have studied the microscopic structure and the proton conductivity of sol–gel derived organic–inorganic membranes by means of thermal and scattering investigations.<sup>3,4</sup> Besides the structure analysis at equilibrium state, the reaction process was also characterized by systematic sampling of the growing clusters in a pregel solution during the gelation by dynamic light scattering and atomic force microscopy (AFM).<sup>19,20</sup> Although emergence of a specific structure is indispensable for the proton pathway, isolation of the conducting domains takes place if crosslinking do not have sufficient role to suppress the concentration fluctuations. For

Additional Supporting Information may be found in the online version of this article.

© 2012 Wiley Periodicals, Inc.

example, macroscopic phase separation was observed if methanol was used as a solvent<sup>3</sup> for the synthesis of the PWA-TesOct composites in spite of the fact that it was a commonly used solvent in the field of the sol-gel synthesis. It is well known that hydrogen bonding and the inductive effect influence the branching structure via the change in the relative reactivity at each reaction front.<sup>26</sup> In the case of tetraethoxysilane, four functional groups can take part in the reaction, where the states of the functional groups, for example, hydrolyzed silanol groups, residual ethoxy groups or generated siloxane bonds can affect the subsequent reactivity and the overall network structure.

As for the PWA-TesOct composites studied so far, the PWA concentration<sup>4</sup> and the preparation temperature dependence<sup>27</sup> of the conductivity, the effect of solvent on the conductivity<sup>3</sup> have been investigated. Although the proton conductivity reached  $\sigma \sim 10^{-2}$  (S/cm), which was practically acceptable value for the fuel-cell applications, leaking of PWA from the hybrid membranes limited further improvement of the proton conductivity, motivating us to permanently introduce acid-groups, for example, sulfonic-acid groups into polymer networks by a silane coupling reaction. However, such acids could take part in the acid-catalyzed reaction itself, resulting in the difficulty to design the suitable structure of proton pathway. Therefore, (3-mercaptopropyl)trimethoxysilane (MPTS) was incorporated into the sol-gel network, followed by postoxidation of the mercapto groups into sulfonic acid<sup>28</sup> after the structure was fixed. Thus, the aim of this article is to fabricate sulfonated hybrid membranes exhibiting the better proton conductivity by the two-step synthesis and also to elucidate the role of catalyst on the proton conductivity.

## EXPERIMENTAL

### Samples

The sol-gel precursor, 1,8-bis(triethoxysilyl)octane (TesOct),  $(\text{OC}_2\text{H}_5)_3\text{-Si-(CH}_2)_8\text{-Si-(OC}_2\text{H}_5)_3$ , was synthesized<sup>29</sup> by hydrosilylation of octadiene with triethoxysilane in toluene in the presence of the Karstedt catalyst<sup>30,31</sup> at 20°C. Octadiene (Alfa Aesar), triethoxysilane (Tokyo Chemical Industry) and toluene (Wako Chemical, Japan), and Karstedt catalyst (Umicore Japan) were used as-received. TesOct was purified at least twice by reduced pressure distillation.

The mixture of 6-functional TesOct and tri-functional (3-mercaptopropyl)trimethoxysilane (MPTS) in isopropanol (IPA) and water lead to a branched hybrid network via the hydrolysis and condensation reactions. The resulting structure strongly depends on the type of catalysts. For example, when an acid catalyst is used, a weakly branched network is obtained because of the rapid hydrolysis and slow condensation. Conversely, highly branched clusters are obtained if a basic catalyst promotes the nucleophilic reaction. In this study, two types of acids are used, that is, one is regular acid, hydrochloric acid (HCl) and the other is superacid, PWA. Note that PWA has a role not only as a catalyst but also as a proton conductor as described in our previous works. In this study, sulfonic-acid groups are introduced in the network by oxidation of mercapto groups of MPTS, thereby PWA is unneces-

sary or only used as a superacid catalyst. Hereafter, the HCl and PWA catalyzed hybrids are, respectively, abbreviated to HCl-Sul-TesOct and PWA-Sul-TesOct.

PWA (Aldrich), IPA (Wako Chemical, Japan), MPTS (Shin-etsu Chemical), 1 N hydrochloric acid (HCl, Wako Chemical, Japan), and hydrogen peroxide ( $\text{H}_2\text{O}_2$ , Wako Chemical, Japan) were used as received. The reaction was initiated by mixing a TesOct/MPTS/IPA solution into either PWA/IPA or HCl/IPA solution at 20°C. After vigorous stirring, the solution was filtered through a Teflon membrane with the pore size 0.25  $\mu\text{m}$  and was poured into a plastic petri dish, followed by an aging period of 24 h. After solidification, the resulting membranes were further aged under saturated vapor pressure at 60°C for another 24 h. The dried membranes were then carefully washed with distilled water for three days. Subsequently, mercapto groups of MPTS were oxidized into sulfonic acid groups by immersing the membrane into a saturated hydrogen peroxide solution.<sup>28</sup> The concentration of PWA and MPTS were respectively adjusted in the range  $C_{\text{PWA}} = \frac{[\text{PWA}]}{[\text{TesOct}]} = 0.025\text{--}0.250$  and  $C_{\text{MPTS}} = \frac{[\text{MPTS}]}{[\text{TesOct}]} = 0\text{--}3.73$  where the bracket indicates the molar concentration of each component. The water concentration defined as  $r = \frac{[\text{H}_2\text{O}]}{6[\text{TesOct}]}$  is variable in range 0.25–4. The prescribed volume of 1 N HCl solution was mixed into the reactor batch to adjust the water concentration defined by  $r$  value. The thickness of the sample was in the range 10–160  $\mu\text{m}$ , typically 100  $\mu\text{m}$ .

### Conductivity Measurement

Proton conductivity measurements were performed on a Hioki 3532-80 impedance analyzer coupling with two platinum electrodes placed in a thermostat chamber (Espec, LHL-113) at 80°C/95%RH. The conductivity was determined from the Nyquist plot by an AC impedance method in the range 10 Hz–1 MHz. Warburg impedance was extrapolated to the real axis to obtain the resistance of membranes.<sup>32,33</sup> The measurements were iteratively performed until the impedance reached the plateau value. The humidity and temperature dependences were also examined in range 40–80°C and 45–95%RH, respectively. Because of a stability issue of the membranes, the conductivity for Nafion112<sup>®</sup> was measured at 50°C when the humidity dependence was examined.

### Ion Exchange Capacity Measurements

The ion exchange capacity (IEC) was determined to find the amount of acid groups carried in the hybrid membranes. First, a membrane was soaked in a saturated sodium chloride solution to replace proton by sodium ion. Second, the acid solution was titrated by a sodium hydroxide solution to determine the amount of acid released from the membrane. Subsequently, the dried membrane was weighed to calculate the equivalent weight, EW, defined by

$$\text{EW (g mol}^{-1}\text{)} = \frac{w(\text{g})}{n_{\text{NaOH}}(\text{mol})} \quad (1)$$

where  $w$  and  $n_{\text{NaOH}}$  are weight of the dried membrane and mole of NaOH required to neutralize proton, respectively. Finally, IEC was calculated by

$$\text{IEC}(\text{meq g}^{-1}) = \frac{1000}{\text{EW}} \quad (2)$$

### Water Uptake

The water uptake was calculated as the ratio of the difference between the wet and dry masses to the dry mass of the hybrid film. To obtain the mass of the wet hybrid, the film was quickly weighted on a microbalance after wiping water.

### Normalized Swelling Ratio

The swelling ratio was defined as the ratio of the diameters of the hybrid membrane before and after the oxidization. The obtained swelling ratio was normalized by the diameter of the membrane before oxidization. Note that the variation in the thickness was almost negligible within the error of experimental ranges, and noticeable expansion was only seen for the diameter.

### Atomic Force Microscopy

AFM was operated in tapping mode using a Digital Instruments Multimode AFM, controlled by a Nanoscope IIIa scanning probe microscope controller with an extender module. Commercially available silicon tip with a spring constant of 30–40 N/m, single beam cantilevers of 125  $\mu\text{m}$  long and a typical radius of curvature in the range 5–10 nm was used at the resonance frequencies ranging from 310 to 340 kHz depending on cantilever. Both topography and phase images with various scan sizes 500, 1000, 2000, 4000 nm were collected using tapping mode with a scan rate of 1 Hz in ambient atmosphere at room temperature. These images were transformed into a single master curve of the power-spectra after a second-order background subtraction, fast Fourier transform, and radial averaging by homemade software.<sup>4</sup>

### Thermogravimetric Analysis

Thermogravimetric analysis (TGA) was conducted using a TGA2950 (TA Instruments thermogravimetric analyzer) with high-resolution mode. The weight of samples was in the range 5–9 mg. Nitrogen was used as a purge gas. The heating rate was dynamically varied in response to the changes in the decomposition rate of the sample so as to improve the resolutions of the weight change. Maximum ramp heating rate was set at 20°C/min.

### Fourier Transform Infrared Spectroscopy

Fourier transform infrared spectroscopy (FTIR) measurements were performed on a Perkin-Elmer Spectrum GX system equipped with an attenuated total reflection (ATR) attachment. The ATR spectra were collected in the wave number ranging from 650 to 4000  $\text{cm}^{-1}$  with a resolution of 4  $\text{cm}^{-1}$ . The background spectra including the absorption of moisture and carbon dioxide were obtained by measuring the absorption of an empty ATR crystal used as reference.

## RESULTS AND DISCUSSION

Figure 1 shows the proton conductivity,  $\sigma$ , for a series of the Sul-TesOct membranes (open markers) as a function of the MPTS concentration,  $C_{\text{MPTS}}$  observed at 80°C/95%RH. The maximum concentration of the MPTS studied here was  $C_{\text{MPTS}} = 3.0$  because the membrane became dissociated in the

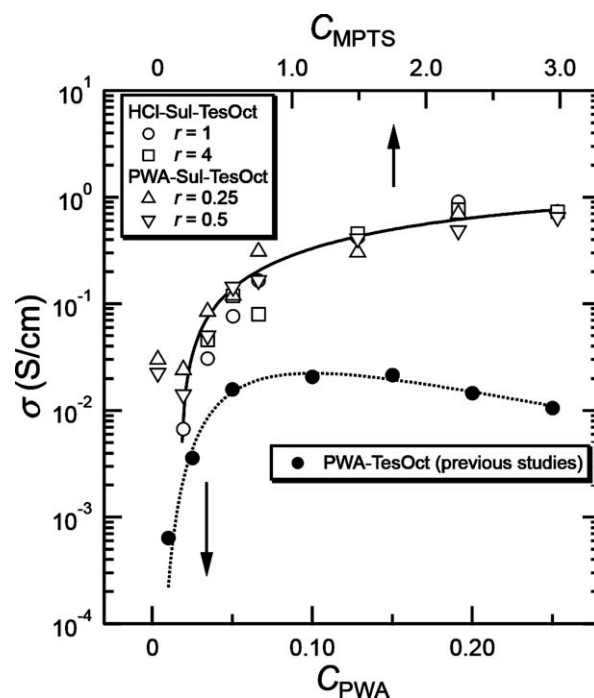


**FIGURE 1** The proton conductivity,  $\sigma$ , for a series of the Sul-TesOct membranes (open markers) and PWA-TesOct membranes (solid markers), respectively, as functions of  $C_{\text{MPTS}}$  and  $C_{\text{PWA}}$  observed at 80°C/95%RH.

hydrogen peroxide solution. The results for the conventional PWA-TesOct membranes without MPTS were also plotted in closed markers for comparison. The solid and dotted lines are guided for the eyes. In the case of the conventional PWA-TesOct membranes, it has already known that  $\sigma$  exhibits a maximum around  $C_{\text{PWA}} = 0.1$  due to competition between the moderate domain growth and aggregation of PWA. As seen from the figure, the (HCl- or PWA-)Sul-TesOct membranes systematically exhibited the proton conductivity higher than these for the PWA-TesOct membranes regardless of the range of the MPTS concentration. The significant improvement of the proton conductivity was achieved over the wide range of  $C_{\text{MPTS}}$  and the maximum conductivity  $\sigma = 0.91(\text{S}/\text{cm})$  was obtained for  $C_{\text{MPTS}} = 2.24$ . Surprisingly, the behavior seemed to be invariant to the catalysis used (HCl or PWA) for the network formation.

Figure 2(a) shows the IEC as a function of  $C_{\text{MPTS}}$ . IEC increased with  $C_{\text{MPTS}}$ , suggesting the effective incorporation of sulfonic acid groups into the network. If we simply assume that fully oxidized MPTS is incorporated in the network without loss and monomers are fully hydrolyzed, the dashed line is expected from a simple stoichiometric calculation. Obviously, the line systematically overestimates the IEC values, probably due to the simplified assumption. As all the monomers can be treated as fully hydrolyzed condition, particularly for the acid catalyzed system, the discrepancy might be attributed to incomplete oxidization of the SH groups or unsuccessful incorporation of MPTS monomer. As described later, the actual composition can be estimated by peak

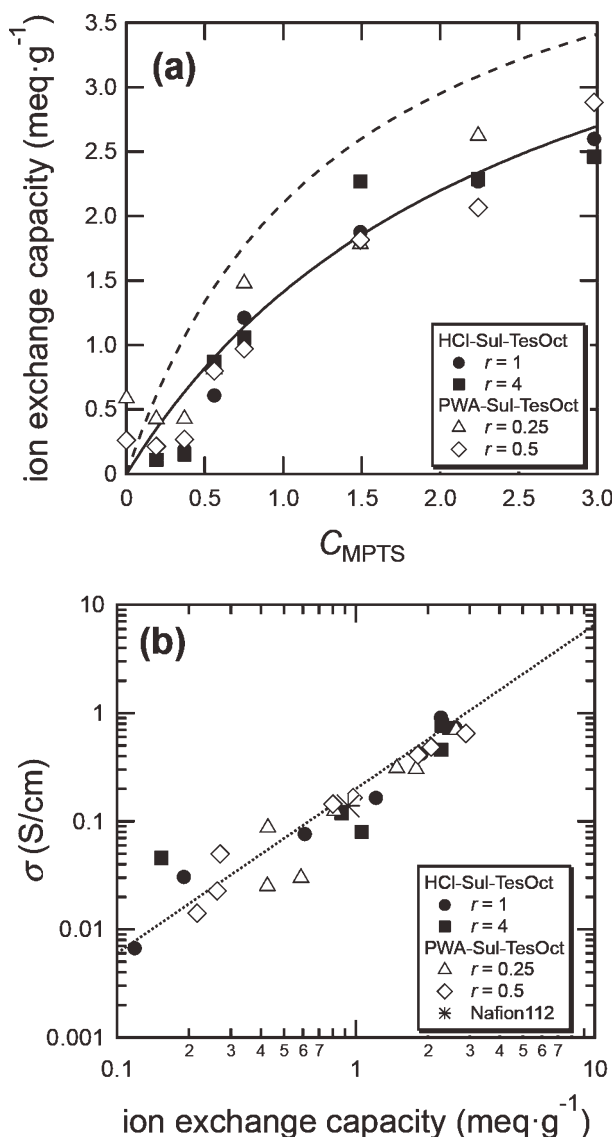


**FIGURE 2** (a) The IEC as a function of  $C_{\text{MPTS}}$ . The dashed and solid lines are the theoretical prediction (See context). (b) The double logarithmic plot of  $\sigma$  versus IEC observed at 80°C/95%RH. The dotted line is the best fit with a power-law function.

separation of the TGA data. By taking into account the amount of MPTS successfully incorporated into the network, the predicted curve nicely agreed with the experimental data as indicated by the solid line. It is also noted that IEC for the PWA-Sul-TesOct membranes at  $C_{\text{MPTS}} = 0$  has a finite value because of the conductivity of PWA itself. The IECs were almost independent on the catalysts similar to the result of the conductivity obtained above. Then, the double logarithmic plot of  $\sigma$  versus IEC is shown in Figure 2(b). As indicated by the dotted line, the data well falls on a single master curve with a power-law with an exponent of  $1.52 \pm 0.16$  which is smaller than 2.0 predicted by the three-dimensional (3D) percolation theory.<sup>34</sup> The figure indicates that the conductivity can be determined almost all by the IEC measurements at least 95%RH.

Figure 3 shows the relative humidity dependence on  $\sigma$  with different  $C_{\text{MPTS}}$  obtained, respectively, (a) for the HCl-Sul-TesOct and (b) the PWA-Sul-TesOct membranes. The results for Nafion112<sup>®</sup> were also plotted in the figures. The proton conductivity decreased with decreasing the relative humidity for all the data. However, the reduction of  $\sigma$  was much smaller for the HCl-Sul-TesOct membranes compared to those for PWA-Sul-TesOct. In the case of the HCl-Sul-TesOct membranes, particularly for  $C_{\text{MPTS}} = 2.98$ ,  $\sigma$  was much larger than Nafion112 throughout the humidity range studied here. Conversely, for the PWA-Sul-TesOct membrane, although  $\sigma$  ( $C_{\text{MPTS}} = 2.24$ ) at 95%RH exhibited a pronounced value of  $\sigma = 0.3$  (S/cm) as indicated in Figure 3(b), the low humidity performance was fairly poor compared with those for the HCl-Sul-TesOct or Nafion112. In other words, comparing the HCl to the PWA catalyzed membranes,  $\sigma$  at the water-saturated condition are almost equivalent, whereas those at the lower humidity condition are completely different.

It is well known that there are two types of mechanism for the proton transfer; that is, the vehicle mechanism and the Grotthuss mechanisms.<sup>35</sup> The former is based on the direct transportation of proton as oxonium ions, whereas the latter originates from the exchange of proton between oxonium ion and water. The Grotthuss mechanism requires less activation energy thereby suitable for the better proton conduction. Note that apparent activation energy could be larger at high temperature because of the swelling (less local density of ion). Thus, the obtained slopes may not represent the correct activation energy. Although the results are not shown here, the activation energy estimated by the Arrhenius plot (irrespective to the fitting range) was around 20–50 kJ mol<sup>-1</sup>, which is close to the value reported in the literature.<sup>36</sup> Therefore, Grotthuss mechanism could mainly contribute to the proton transportation. To understand the roles of low-humidity in the proton conductivity, the swelling properties of the membranes were examined. Figure 4(a) shows the water uptake of the membranes prepared with HCl (solid symbols) and PWA (open symbols) catalysts. As seen from the figure, the PWA-catalyzed membranes contained more water molecules than the HCl catalyzed membranes. Therefore, it is expected that the former membranes swell more than the latter one. However, as evidenced from the swelling ratio measurement shown in Figure 4(b), the normalized swelling ratio, which is defined as the ratio of the diameters of the membrane before and after the oxidization in the equilibrium swelling state, is systematically higher for the HCl-Sul-TesOct membranes compared to the PWA-Sul-TesOct membranes. From this experimental evidence, it is expected that the PWA-Sul-TesOct membranes have porous and rigid structures compared to the HCl-Sul-TesOct membranes as schematically illustrated in Figure 4(c). For the HCl-Sul-TesOct membranes, the gel-like structure may be formed as expected from pronounced swelling and moderate water uptake. This is easily understood from the fact the acid-catalyzed reaction leads to a weakly branched network immersed in a solvent.<sup>37</sup> When PWA, a superacid is used, the chain extension might occur drastically in preference to

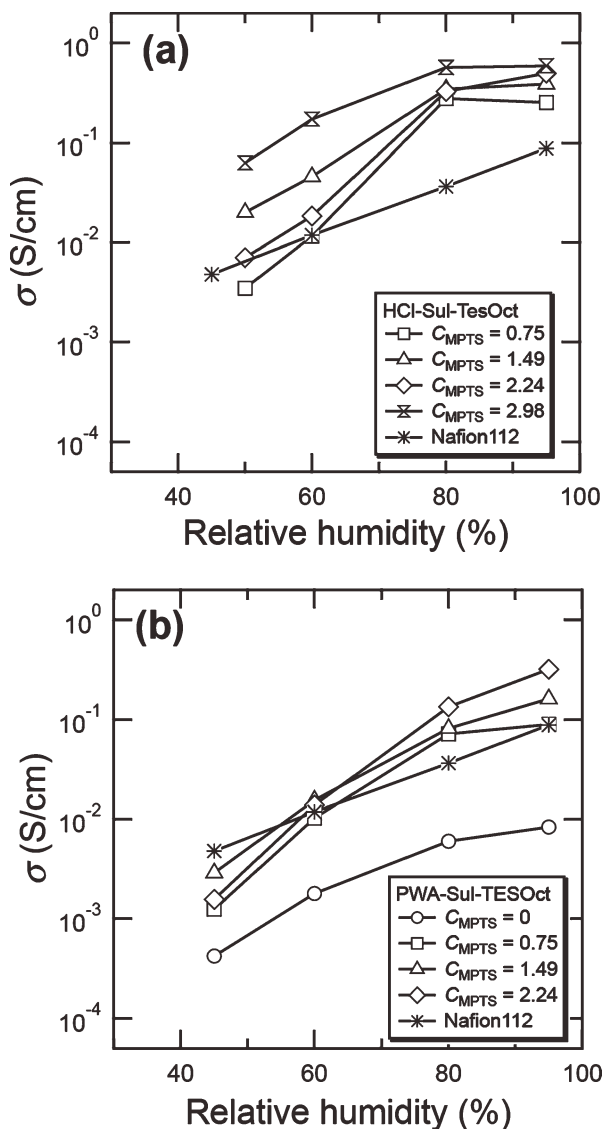
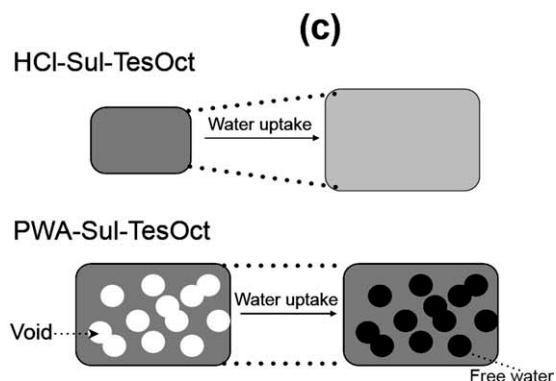
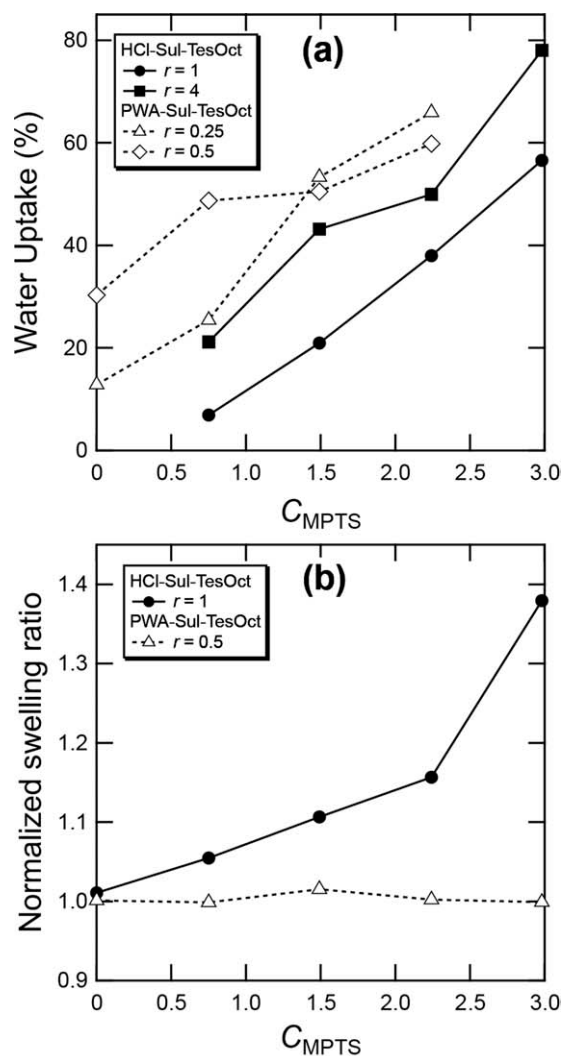


**FIGURE 3** The relative humidity dependence on  $\sigma$  with different  $C_{MPTS}$  obtained, respectively, (a) for the HCl-Sul-TesOct and (b) the PWA-Sul-TesOct membranes at 80°C.

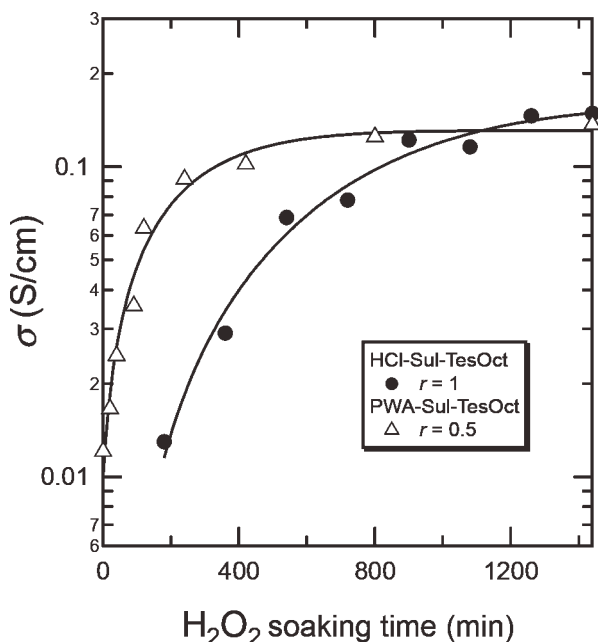
crosslinking of tetrafunctional monomers, leading to instability of the system and the domain structure would noticeably grow.

Figure 5 shows the oxidation time dependence on the proton conductivity. The HCl- and PWA-Sul-TesOct membranes were divided into several pieces to prepare the samples with the different oxidation time. As can be seen from the figure, the data for the PWA-Sul-TesOct membranes reached a plateau value at the shorter soaking time. From all above experimental findings, one can speculate that the porosity of the membrane was much larger for the PWA-Sul-TesOct membranes than those for HCl-Sul-TesOct. Although the SEM micrographs showed the structure (not shown here), further investigation is required to ensure the hypothesis. It is noted that the proton conductivity reached plateau values at 800 and

1200 min, respectively, for HCl- and PWA- Sul-TesOct membranes. Therefore, all the conductivity measurements shown above were performed after immersion of the membranes more than 1 day.



**FIGURE 4** (a) The water uptake of the membranes (b) normalized swelling ratio, and (c) the schematic model of the membrane structures.



**FIGURE 5** The oxidation time dependence on the proton conductivity  $\sigma$  observed at 80°C.

To clarify the structural difference between the HCl- and PWA- catalyzed Sul-TesOct membranes, TGA were carried out. The weight loss curve (weight  $W$  vs. temperature  $T$ ) was differentiated with respect to the temperature.  $dW/dT$  exhibited two peaks around at 350°C (region I) and at 500°C (region II) as shown in Figure 6(a,b). The former corresponds to the dissociation of MPTS, whereas the latter corresponds to that of the highly condensed block<sup>38</sup> made of TesOct, which is confirmed by independent FTIR measurements. It should be noted that there is another peak in the region I probably attributed to the different number (i.e., singlet, doublet, or triplet) of siloxane links in MPTS. Subsequently, peak separation was carried out to obtain the amplitude and the locations of the three peaks. The curve was well reproduced by the sum of three Lorentzian functions. As indicated by the arrow, the peak heights in region I increased with  $C_{\text{MPTS}}$  because of incorporation of MPTS into the network. Conversely, those in region II decreased with  $C_{\text{MPTS}}$ , indicating that the highly condensed cage-like structures made of 6-functional TesOct became less branched due to incorporation of trifunctional MPTS. For both systems, all the peaks became broadened with  $C_{\text{MPTS}}$ . However, noticeable peak shift was only observed for the PWA-Sul-TesOct samples as indicated in the region II in Figure 6(b).

Without MPTS, it has been already known that the PWA catalyst leads to a rigid structure of TesOct network having high thermal stability.<sup>4</sup> The dissociation temperature of the previously reported PWA-TesOct membranes appeared around 500–520°C, which was fairly larger than that of the conventional HCl-TesOct membranes (490°C). This is probably due to the high charge density of superacid, PWA, which sufficiently promotes the condensation reaction of the silanol

groups. However, the reaction process accompanying three functional MPTS under superacid environment becomes tricky. If the concentration fluctuations are not well suppressed by crosslinks due to the presence of trifunctional species, the system becomes unstable as large molecular-weight species are formed, leading to phase separation or formation of the porous structures.

Subsequently, the ratio of the peak areas attributed to MPTS and TesOct was calculated to evaluate the MPTS composition. Figure 6(c) shows the composition of MPTS obtained by TGA,  $r_{\text{TGA}}$ , versus the feed composition,  $r_{\text{feed}}$ . As the result of nonleast squares fitting, slope was about 0.55 irrespective of the type of catalyst, indicating that 55% of MPTS monomer was actually incorporated into the TesOct network. By taking

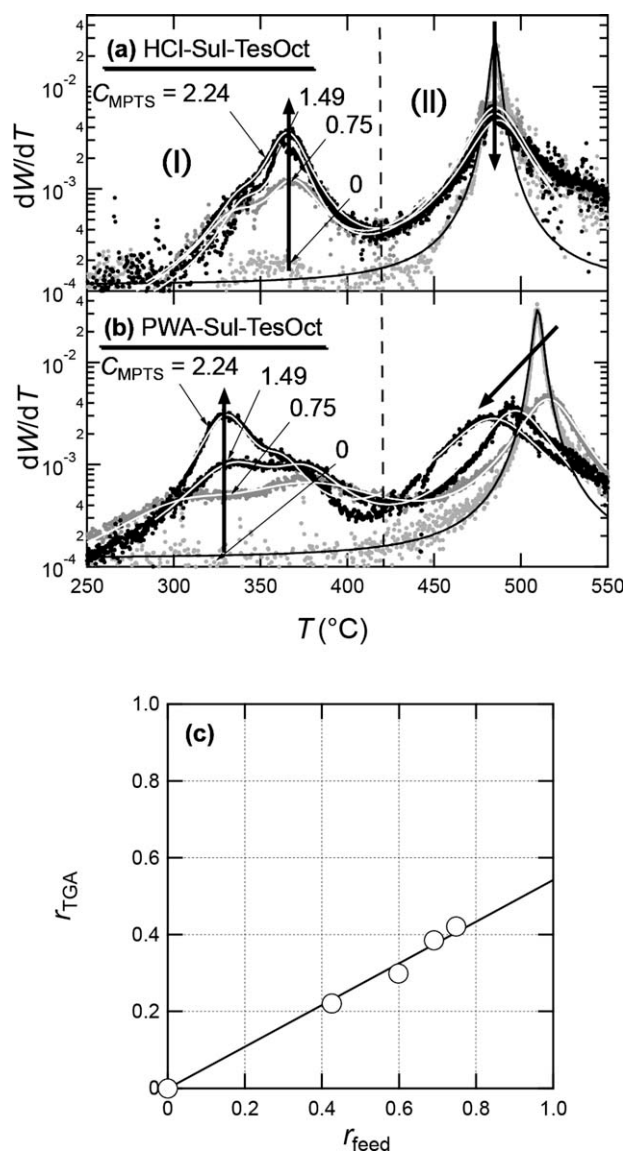


**FIGURE 6** Temperature derivative of the weight loss  $dW/dT$  evaluated by TGA obtained for the (a) HCl and (b) PWA-Sul-TesOct membranes. The solid lines indicate the best fit by three multiple Lorentzian functions. (c)  $r_{\text{TGA}}$  versus  $r_{\text{feed}}$ .

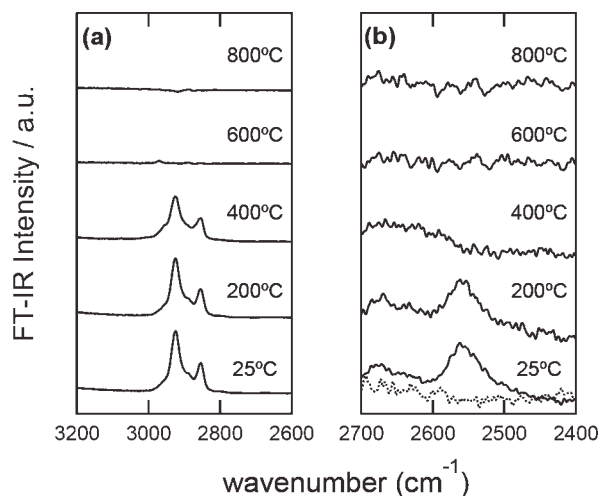


**FIGURE 7** FTIR spectra for the HCl-Sul-TesOct membranes before the oxidation procedure indicating the presence of (a) organic bridge of TesOct and (b) mercapto group of MPTS. The spectra were acquired after TGA under different destination temperatures. The dotted line shows the data after the oxidation procedure.

the real composition instead of the feed value into account, we obtained the good agreement between the experimental and predicted lines of IEC as shown in Figure 2(a).

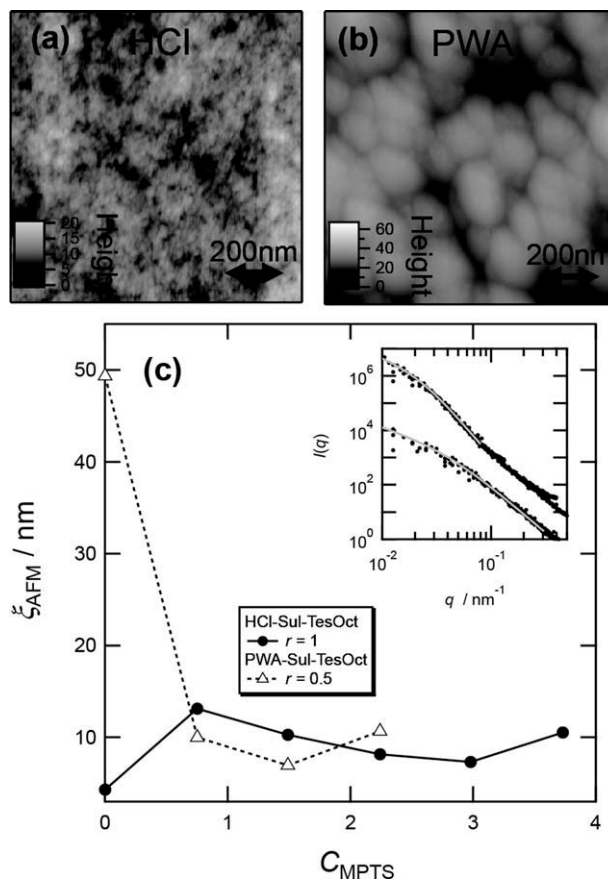
Figure 7(a,b) show FTIR spectra for the HCl-Sul-TesOct membranes before the oxidation procedure. The spectra indicate the presence of (a) organic bridge of TesOct and (b) mercapto group of MPTS, which are respectively evidenced by the peaks appeared at  $2900\text{ cm}^{-1}$ ;  $(\text{CH}_2)_8$  and  $2550\text{ cm}^{-1}$ ;  $(\text{CH}_2)_3\text{SH}$ . The spectra were acquired after TGA under different destination temperatures where disappearance of the corresponding peaks on heating was clearly confirmed. Although the peak associated to the sulfonic acid group overlapped with other peaks, it was found that disappearance of the MPTS peak after oxidation was clearly observed as indicated by the dotted curve in Figure 7(b), suggesting most of the SH groups are transformed into the sulfonic acid groups at least in the detectable level of the FTIR measurements.

Figure 8(a) shows the AFM height morphology obtained for the (a) HCl and (b) PWA-Sul-TesOct membranes at  $C_{\text{MPTS}}=0$ . As can be seen from the images, the latter has the larger domain structure than the former one. To quantitatively evaluate the structural difference, the 1D power spectra were evaluated from the height morphology by taking fast Fourier transformation, followed by radial average. As shown in Figure 7(b), the correlation length  $\zeta$  evaluated from the power spectra (inset) decreased rapidly with  $C_{\text{MPTS}}$  for the PWA-Sul-TesOct membranes, whereas those for the HCl-Sul-TesOct was rather invariant. The behavior was quite similar to that obtained for the characteristic temperature of the membranes evaluated by TGA (region II in Fig. 6). Although the AFM results indicated that addition of MPTS led to dissociation of the rigid structure of TesOct precursor in the PWA-

Sul-TesOct membranes, it was quite difficult to find the difference of the structures between PWA- and HCl-Sul-TesOct membranes for the larger  $C_{\text{MPTS}}$  only from the AFM analysis. Conversely, the TGA results suggested that the low thermostable species were dominant (region I in Fig. 6) in the PWA-Sul-TesOct membranes. Thus, it provides an insight for the structure of PWA-Sul-TesOct membranes where the chemical bonding is weaker than those for the HCl-Sul-TesOct. In general, multifunctional precursor such as TesOct with a super acid would lead to a well-developed network. However, when trifunctional coupling agent is incorporated into the network, the concentration fluctuations grow so rapidly because of the loose structure involving less junction points, resulting in macrophase separation. This suggests that superacid PWA is not always the best catalyst for this particular purpose, instead a normal acid like HCl could produce a gel like structure suitable for the better proton conduction.

### CONCLUSIONS

Sol-gel derived hybrids containing sulfonic acid groups were fabricated to obtain thermostable proton conductive membranes. The conductivity reached  $\sigma = 0.9\text{ (S/cm)}$ , which was



**FIGURE 8** The AFM height morphology obtained for the (a) HCl and (b) PWA-Sul-TesOct membranes at  $C_{\text{MPTS}} = 0$ . (c) The correlation length  $\zeta$  versus  $C_{\text{MPTS}}$ . The power spectra were shown in the inset.

respectively two orders and one order higher than the previously reported values for the similar hybrids and Nafion 112. Beside the high conductivity at the high humidity condition, the conductivity depends on the type of catalysts particularly at the lower humidity. When PWA was used as a catalyst, the conductivity became poor with decreasing the humidity, which was attributed to the porous structure where water molecules are easily released on drying. The swelling ratio, water uptake, thermo-gravimetry analysis, and AFM results supported the hypothesis. Although multifunctional monomers such as bis(triehoxyisilyloctane) have potential to produce versatile structures, the catalyst used here plays an important role to control the mesostructures suitable for the better proton conduction. Such differences are not realized from the IEC measurements, suggesting the importance to carry out the structural or thermal analysis to understand the mechanism of the proton conduction.

#### ACKNOWLEDGMENTS

This work is supported by Grant-in-Aid, No. 18750190 (for T. N.) and Grant-in-Aid for Scientific Research on Priority Area, "Soft Matter Physics" (No. 463/19031018) from the Ministry of Education, Science, Sports, Culture, and Technology. The authors thank Shinji Sugihara, Department of Applied Chemistry and Biotechnology, University of Fukui, for the valuable discussion.

#### REFERENCES AND NOTES

- 1 Shea, K. J.; Loy, D. A. *Chem. Mater.* **2001**, *13*, 3306–3319.
- 2 Loy, D. A.; Carpenter, J. P.; Alam, T. M.; Shaltout, R.; Dorhout, P. K.; Greaves, J.; Small, J. H.; Shea, K. J. *J. Am. Chem. Soc.* **1999**, *121*, 5413–5425.
- 3 Sato, H.; Norisuye, T.; Takemori, T.; Tran-Cong-Miyata, Q.; Nomura, S. *Polymer* **2007**, *48*, 5681–5687.
- 4 Nakanishi, T.; Norisuye, T.; Sato, H.; Takemori, T.; Tran-Cong-Miyata, Q.; Nomura, S.; Sugimoto, T. *Macromolecules* **2007**, *40*, 4165–4172.
- 5 Miyatake, K.; Tombe, T.; Chikashige, Y.; Uchida, H.; Watanabe, M. *Angew. Chem. Int. Ed.* **2007**, *46*, 6646–6649.
- 6 Miyatake, K.; Watanabe, M. *J. Mater. Chem.* **2006**, *16*, 4465–4467.
- 7 Takimoto, N.; Wu, L.; Ohira, A.; Takeoka, Y.; Rikukawa, M. *Polymer* **2009**, *50*, 534–540.
- 8 Tung, S. P.; Hwang, B. J. *J. Mater. Chem.* **2005**, *15*, 3532–3538.
- 9 Uma, T.; Nogami, M. *Anal. Chem.* **2008**, *80*, 506–508.
- 10 He, S. L.; Yu, J. J.; Li, C. H.; Fang, J. H.; Xu, J.; Guan, R. *Polym. Eng. Sci.* **2011**, *51*, 264–271.
- 11 Lee, C. H.; Wang, Y. Z. *J. Polym. Sci. Part A: Polym. Chem.* **2008**, *46*, 2262–2276.
- 12 Won, J.; Park, H. H.; Kim, Y. J.; Choi, S. W.; Ha, H. Y.; Oh, I.-H.; Kim, H. S.; Kang, Y. S.; Ihn, K. *J. Macromolecules* **2003**, *36*, 3228–3234.
- 13 Serpico, J. M.; Ehrenberg, S. G.; Fontanella, J. J.; Jiano, X.; Perahia, D.; McGrady, K. A.; Sanders, E. H.; Kellogg, G. E.; Wnek, G. E. *Macromolecules* **2002**, *35*, 5916–5921.
- 14 Sel, O.; Soules, A.; Ameduri, B.; Boutevin, B.; Laberty-Robert, C.; Gebel, G.; Sanchez, C. *Adv. Funct. Mater.* **2010**, *20*, 1090–1098.
- 15 Bae, B.; Miyatake, K.; Watanabe, M. *Macromolecules* **2010**, *43*, 2684–2691.
- 16 Li, N. W.; Liu, J.; Cui, Z. M.; Zhang, S. B.; Xing, W. *Polymer* **2009**, *50*, 4505–4511.
- 17 Peckham, T. J.; Schmeisser, J.; Rodgers, M.; Holdcroft, S. *J. Mater. Sci.* **2007**, *17*, 3255–3268.
- 18 Miyatake, K.; Chikashige, Y.; Higuchi, E.; Watanabe, M. *J. Am. Chem. Soc.* **2007**, *129*, 3879–3887.
- 19 Takata, Y.; Norisuye, T.; Hirayama, S.; Takemori, T.; Tran-Cong-Miyata, Q.; Nomura, S. *Macromolecules* **2007**, *40*, 3773–3778.
- 20 Aoki, Y.; Norisuye, T.; Tran-Cong-Miyata, Q.; Nomura, S.; Sugimoto, T. *Macromolecules* **2003**, *36*, 9935–9942.
- 21 Rollet, A. L.; Diat, O.; Gebel, G. *J. Phys. Chem. B* **2002**, *106*, 3033–3036.
- 22 Gierke, T. D.; Munn, G. E.; Wilson, F. C. *J. Polym. Sci. Polym. Phys. Ed.* **1981**, *19*, 1687–1704.
- 23 Gebel, G.; Lambard, J. *Macromolecules* **1997**, *30*, 7914–7920.
- 24 Ma, X. H.; Zhang, C. J.; Xiao, G. Y.; Yan, D. Y.; Sun, G. M. *J. Polym. Sci. Part A: Polym. Chem.* **2008**, *46*, 1758–1769.
- 25 Mikami, T.; Miyatake, K.; Watanabe, M. *J. Polym. Sci. Part A: Polym. Chem.* **2011**, *49*, 452–464.
- 26 Brinker, C. J.; Scherer, G. W. *Sol-Gel Science*; Academic Press: London, **1990**.
- 27 Norisuye, T.; Ikezawa, Y.; Takemori, T.; Tran-Cong-Miyata, Q.; Nomura, S. *Kobunshi Ronbunshu* **2008**, *65*, 716–729.
- 28 Daiko, Y.; Katayama, H.; Araki, T.; Mineshige, A.; Kobune, M.; Yusa, S.; Yazawa, T.; Nagasaka, K.; Murata, S.; Matsumoto, S.; Koiwai, A.; Konomi, I. *J. Phys. Chem. C* **2009**, *113*, 1891–1895.
- 29 Loy, D. A.; Jamison, G. M.; Baugher, B. M.; Myers, S. A.; Assink, R. A.; Shea, K. J. *Chem. Mater.* **1996**, *8*, 656–663.
- 30 Karstedt, B. D. U.S. Patent No. 3,775,492, **1973**.
- 31 Oviatt, H. W., Jr.; Shea, K. J.; Small, J. H. *Chem. Mater.* **1993**, *5*, 943–950.
- 32 Kim, J. D.; Honma, I. *Electrochim. Acta* **2004**, *49*, 3429–3433.
- 33 Lefebvre, M. *Chem. Mater.* **1999**, *11*, 262–268.
- 34 Stauffer, D. *Introduction to Percolation Theory*; Taylor & Francis: London, **1985**.
- 35 Nogami, M.; Daiko, Y.; Akai, T.; Kasuga, T. *J. Phys. Chem. B* **2001**, *105*, 4653–4656.
- 36 Onizuka, H.; Kato, M.; Shimura, T.; Sakamoto, W.; Yogo, T. *J. Sol-Gel Sci. Technol.* **2008**, *46*, 107–115.
- 37 Norisuye, T.; Inoue, M.; Shibayama, M.; Tamaki, R.; Chujo, Y. *Macromolecules* **2000**, *33*, 900–905.
- 38 Ni, Y.; Zheng, S. X. *Chem. Mater.* **2004**, *16*, 5141–5148.